

Ultrasound-Induced Gradient Crystals Observed by High-Energy X-rays

K.-D. LISS,^{a*} A. MAGERL,^b A. REMHOF^{b,c} AND R. HOCK^d

^aEuropean Synchrotron Radiation Facility, BP 220, F-38043 Grenoble CEDEX, France, ^bInstitut Max von Laue–Paul Langevin, BP 156, F-38042 Grenoble CEDEX, France, ^cRuhruniversität Bochum, D-44780 Bochum, Germany, and ^dMineralogisches Institut der Universität Würzburg, Am Hubland, D-97074 Würzburg, Germany. E-mail: liss@esrf.fr

(Received 5 July 1996; accepted 22 October 1996)

Abstract

High-energy X-ray scattering (90 keV) has been performed at the high-energy beamline ID15 at the European Synchrotron Radiation Facility, Grenoble, on perfect Si crystals excited by compressional ultrasound waves in the [111] direction. Two-dimensional intensity maps of the $\bar{3}51$ Bragg peak reveal a purely longitudinal distortion of the lattice with respect to the applied distortion field, which is, for the present scattering geometry, inclined by 72° to the diffraction vector. A maximum gain factor of 50 for the diffracted intensity is observed for the strongest sound excitation. A quantitative analysis of the line shape by a transfer-matrix method shows the transition from the diffraction behavior of an ideal crystal towards a crystal slightly deformed by internal stresses.

1. Introduction

In Bragg optics, one distinguishes between transversal and longitudinal variations of the reciprocal-lattice vector \mathbf{G} with respect to the diffraction vector \mathbf{Q} . The first case is represented by a so-called mosaic crystal, which is macroscopically composed of a large number of small crystallites. They are assumed to be statistically oriented within a certain angular distribution around a main direction. The second type is obtained by a crystal with a gradual variation of the lattice parameter while the lattice planes themselves remain parallel. In this case, the scattering from the entire crystal remains coherent. This type is often referred to as a gradient crystal. Both types of crystal show a distinctly different behavior for the transformation of a phase space element on Bragg reflection. The mosaic crystal increases the angular divergence both for the in-plane and the out-of-plane component of the diffracted intensity and, in addition, introduces an energy-direction dispersion. The intensity diffracted by a mosaic crystal is the incoherent sum of the intensities emanating from the individual crystallites. Primary and secondary extinction often limit the performance of monochromator crystals when a monochromator with a broad bandwidth and high reflectivity is to be made. In contrast, a gradient crystal behaves like an optical mirror, *i.e.* the original beam divergencies are maintained and the shape of the selected

volume element is related by a reflection symmetry to the profile of the incoming beam. The entire crystal remains structurally coherent and the intensity is the coherent superposition of diffracted waves for the entire crystal volume (Zachariassen, 1945; Taupin, 1964).

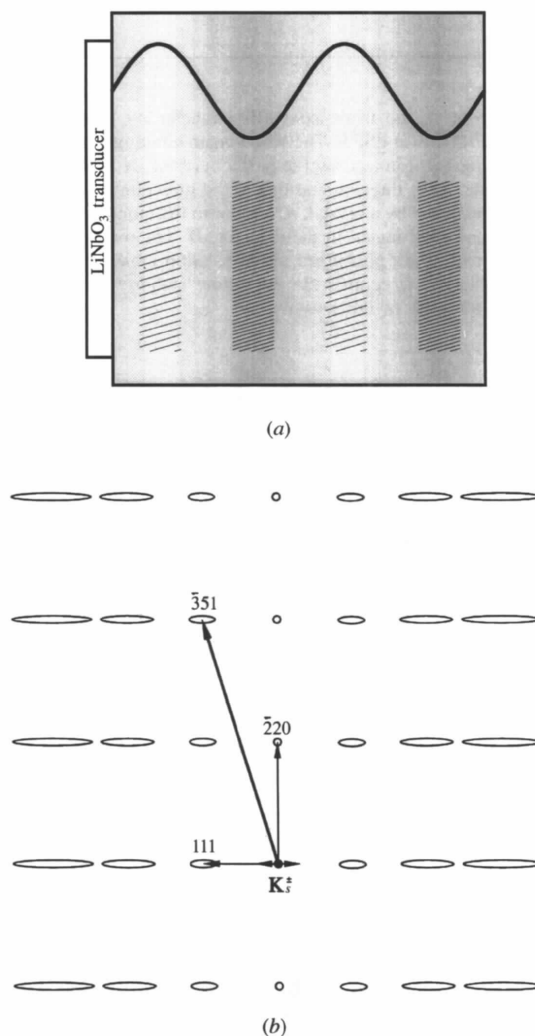


Fig. 1. (a) Real-space and (b) reciprocal-space representation of the scattering geometry: the ultrasonic wave vector \mathbf{K}_s^z is along the [111] direction and the scattering vector is $\bar{3}51$.

Many defects in natural crystals are extensive in size. These structures influence primarily the parallelism of the lattice planes while the lattice parameter is modified to a lesser extent. Thus, crystals with a significant longitudinal gradient need to be made artificially. Indeed, they have been realized by several techniques such as

applying a temperature gradient (Alefeld, 1969), making composition gradients in $\text{Cu}_{1-x}\text{Ge}_x$ (Rustichelli, 1972) and $\text{Si}_{1-x}\text{Ge}_x$ alloys (Magerl, Liss, Doll, Madar & Steichele, 1994; Liss, 1994) or by ultrasound excitation (Kulda, Vrána & Mikula, 1988; Hock *et al.*, 1993).

In the present paper, we consider gradient crystals made by ultrasound excitation in Si. Our emphasis is to study in detail the distortion field *via* a complete mapping of the Bragg intensity. High-energy X-ray diffraction, which has recently become available at third-generation synchrotron sources such as the European Synchrotron Radiation Facility (ESRF), Grenoble, is uniquely suited for this purpose because it combines high penetration power of radiation into material sufficient to analyse sample thicknesses in the cm range with high resolution in reciprocal space.

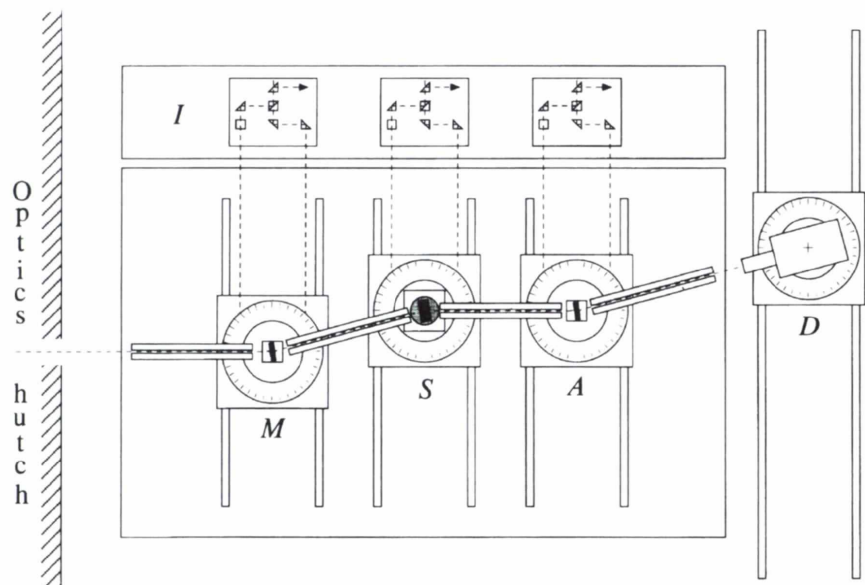


Fig. 2. Layout of the triple-axis diffractometer on the high-energy beamline ID15A at ESRF. The white beam entering from the optics hutch is monochromized by the perfect crystal, *M*, and illuminates the sample, *S*. In three-crystal mode, the direction of the scattered beam is analyzed by a crystal, *A*, similar to the monochromator, and the photons are counted in the detector, *D*. The rotation stages for *M*, *S*, *A* and *D* are positioned *via* translation tables. Three optical interferometers, *I*, control the long time stability of the angular position for each of the crystals.

2. Experimental set-up

We have excited longitudinal ultrasound waves in perfect Si crystals by coupling their surface to a LiNbO_3 transducer with a resonance frequency of ~ 5 MHz. The experiments were performed in the transducer's third-overtone mode at 15.544 MHz, corresponding to an acoustic wavelength of 0.602 mm. With these parameters, a standing wave of 16.5 wavelengths is excited in the 9.93 mm-thick crystal. The geometry is indicated in Fig. 1. The surface normal, and thus the propagation

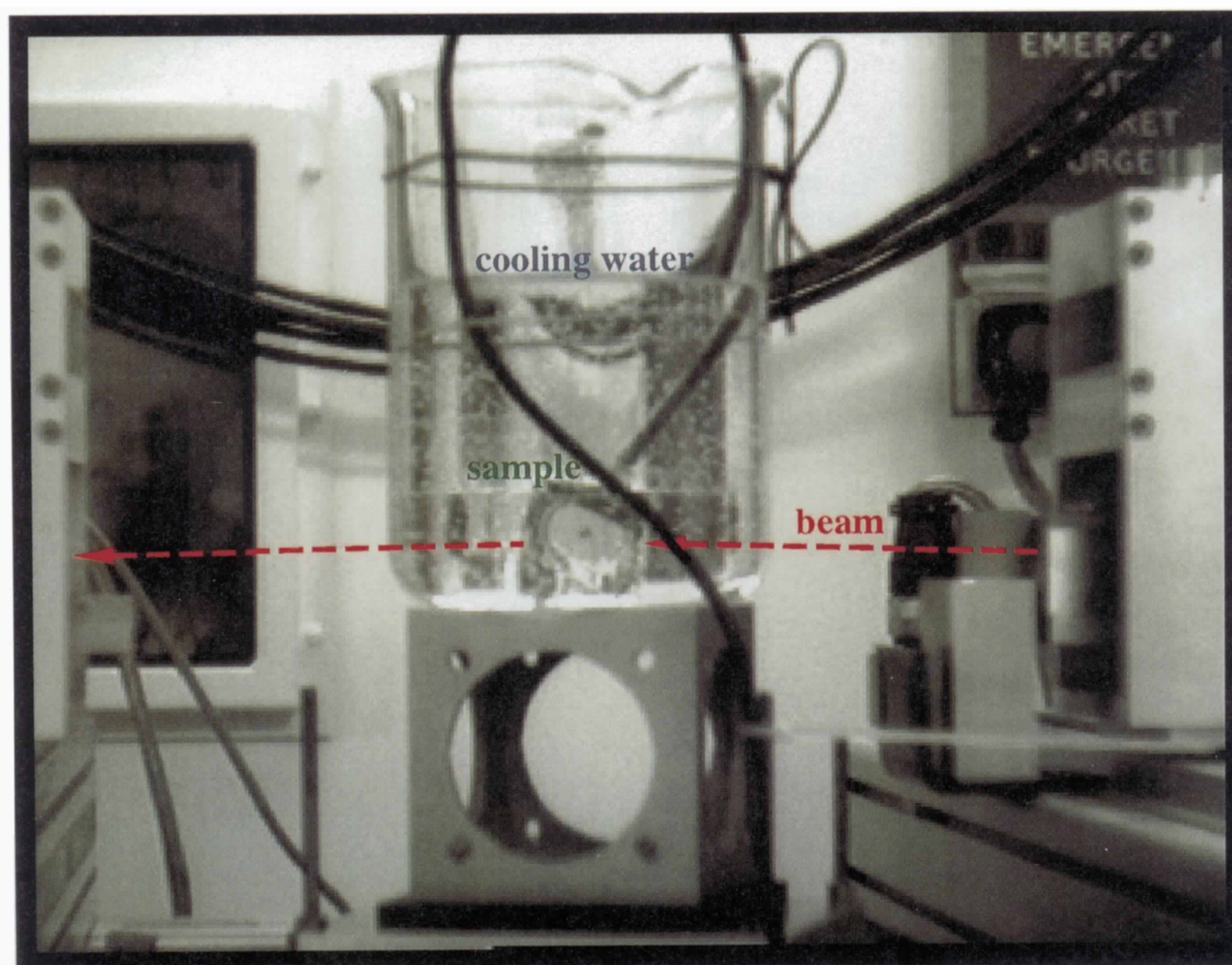


Fig. 3. Photograph of the water jar serving as sample cooling environment. The sample can be seen at the bottom of the glass and has the circular transducer attached to its surface. A coaxial cable connects to the power supply.

vector, \mathbf{K}_s , of the ultrasonic wave coincides with the [111] direction of the crystal.

The crystal was mounted onto the sample axis of the three-axis diffractometer at the high-energy beamline ID15 at ESRF (Suortti & Tschentscher, 1995; Tschentscher *et al.*, 1996). A sketch is given in Fig. 2.

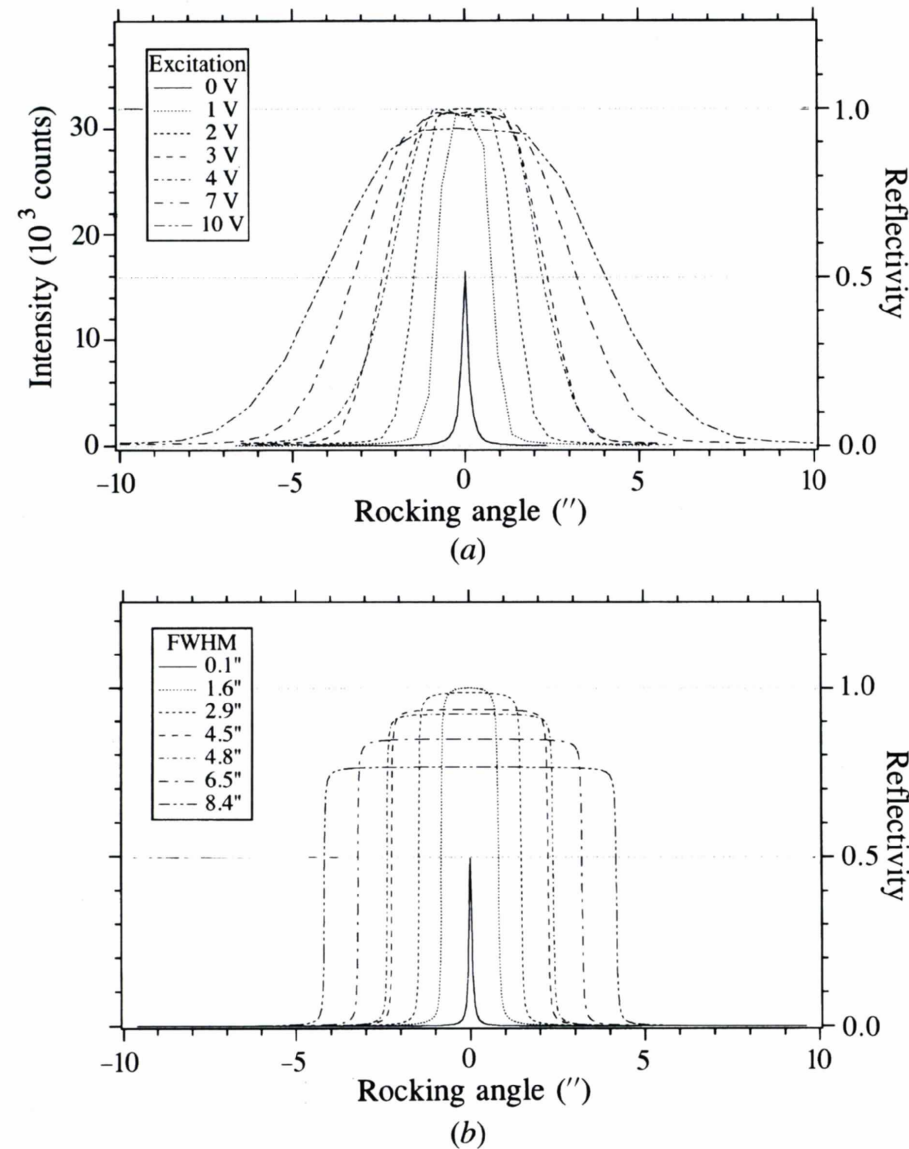


Fig. 4. (a) Measured reflection curves from the ultrasonically excited crystal. The legend shows the control voltage amplitudes, which are a measure of the excitation. (b) Simulations based on a linear gradient crystal model. The only input parameters varied are the full widths at half-maximum taken from the measured curves.

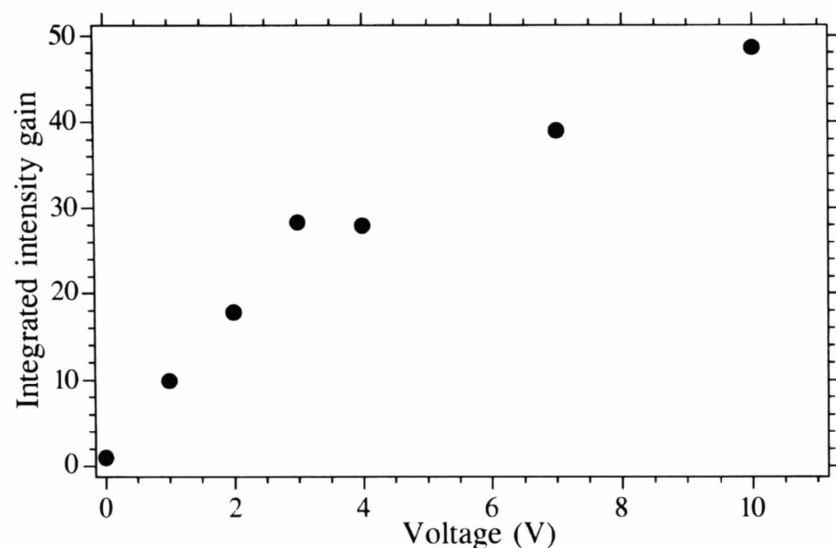


Fig. 5. Integrated intensity gain versus the electric amplitude voltage. The gain first increases linearly with voltage. The discontinuity at 4 V is due to an uncontrolled loss of the acousto-mechanic resonance related to the thermal heat load. The system was stabilized manually before taking the data points of higher sound amplitudes.

Perfect Si crystals of thickness 4 mm were employed as monochromator and analyzer with $\bar{3}51$ reflections in Laue geometry in a non-dispersive set-up on all axes. The X-ray energy chosen was 90 keV. This allows for a high resolution in both longitudinal and transversal directions of reciprocal space of 6.2×10^{-6} and 0.9×10^{-6} , respectively (Neumann, 1991; Liss, 1994; Neumann, Rütt, Bouchard, Schneider & Nagasawa, 1994; Magerl *et al.*, 1995). The absorption length is 21.6 mm, which exceeds the crystal thickness of 9.93 mm. Scans were performed in both two- and three-axis modes to allow fast scanning by integration over the longitudinal component and a two-dimensional analysis of the distribution of scattering vectors, respectively.

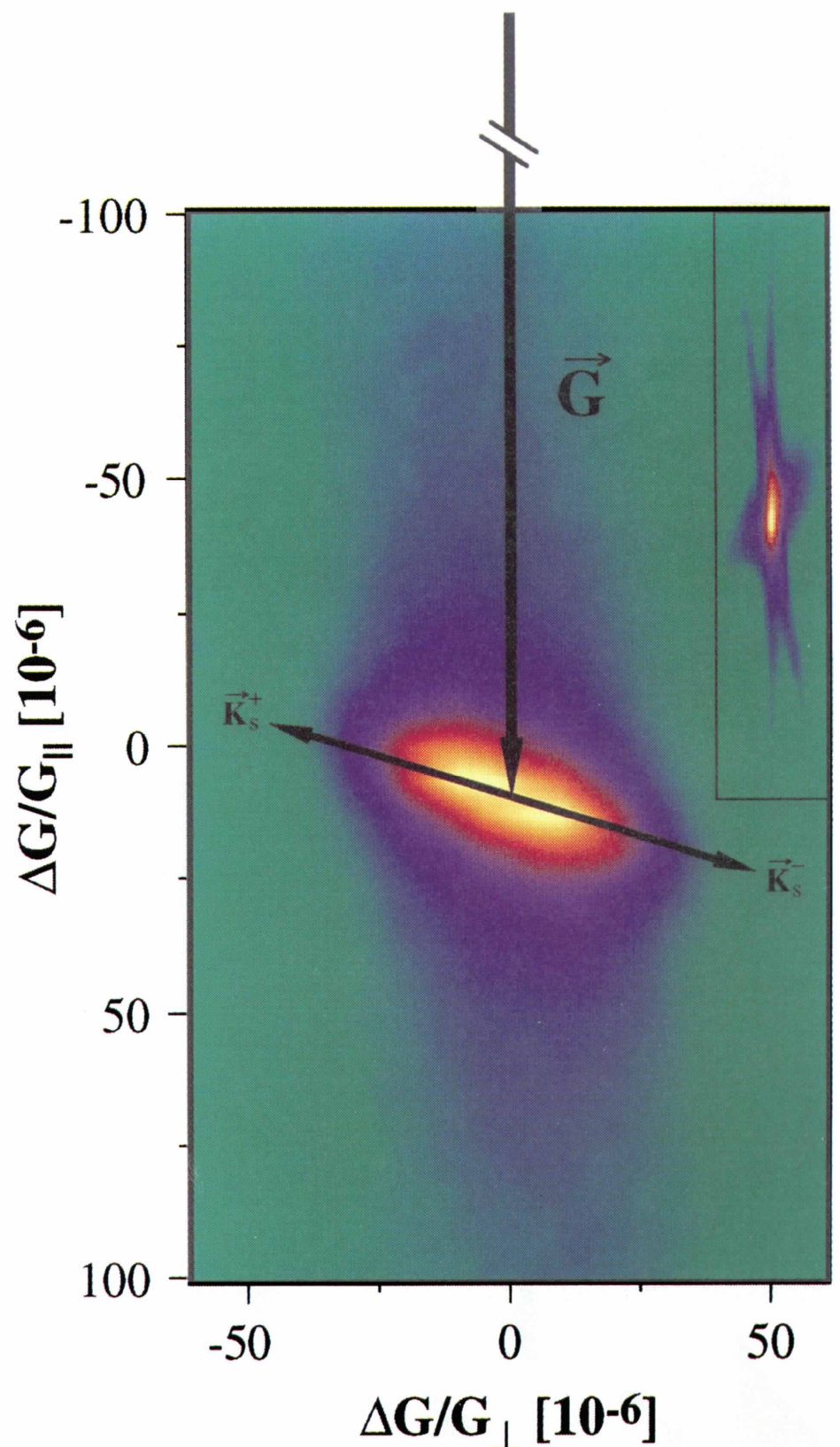


Fig. 6. Two-dimensional reciprocal-lattice vector distribution around the $\bar{3}51$ reflection of the excited crystal. The intensity smears out in the direction of the propagation vectors \mathbf{K}_s^{\pm} of the ultrasonic wave field. The insert shows the instrument resolution.

A crystal excited by an ultrasound transducer in resonance may heat significantly. This may introduce angular shifts for the sample position and the diffraction peak, which must not occur during a scan. It can be avoided by carefully designing an appropriate sample holder. Alternatively, we have put our sample in a water jar with a diameter of 150 mm (Fig. 3). This ensures sufficient cooling and stability, while the transmission of 10% does not affect the present experiment. Obviously, absorption in normal X-ray scattering or diffusion in neutron scattering would prohibit such a solution.

3. Experimental results

Fig. 4 shows a series of rocking curves measured in the two-crystal mode with different excitations of the ultrasound wave amplitude. These first scans have been taken without cooling the sample. It is essential to remain close to the resonance frequency of the transducer-crystal entity to maintain the maximum sound amplitude. Since the resonance is very sharp, it had been necessary to retune the frequency slightly during the individual runs. The narrowest curve has been obtained for the unexcited perfect crystal. With increasing sound amplitude, we first observe a doubling of the peak intensity, which is followed by a widening of the rocking width. Fig. 5 shows the integrated intensities of the rocking profiles in Fig. 4 as a function of the high-frequency voltage at the input of the power amplifier. The slight discontinuity observed in the medium power range is due to the retuning of the resonance as mentioned. For higher power levels, we observe a true onset of saturation of the integrated intensity towards the kinematical limit.

A two-dimensional scan of the reciprocal space around the $\bar{3}51$ reflection taken in the three-crystal mode and at an ultrasound excitation of 10 V is shown in Fig. 6. The insert shows the measured instrument function with the resolution given above. With sound excitation, we clearly see an elongation of the Bragg intensity in a single direction only, which lines up with the [111] direction of the sound propagation while the perpendicular component remains unchanged. The distribution of the reciprocal-lattice vectors is thus modified, as shown in Fig. 1, which proves the longitudinal character of the ultrasonic wave.

4. Evaluation of the diffraction data

The reflection curve of a perfect crystal is described by the dynamical theory of diffraction (Zachariasen, 1945; Rauch & Petrascheck, 1976, 1978; Liss, 1994). At high X-ray energies, absorption can be neglected and the reflection curve for a thick crystal in the Laue geometry is a Lorentzian function with a maximum amplitude of 0.5. The full width at half-maximum for

an Si $\bar{3}51$ rocking curve at 90 keV can be calculated to $0.09''$. Since monochromator and sample use the same reflection, we expect a theoretical full width at half-maximum of $0.192''$. Our experimental line width of $0.203''$ agrees to within 5% of the theoretical resolution. In addition, the measured peak shape harmonizes well with a Lorentzian line shape. This good agreement allows the normalization of the intensity on an absolute scale, as shown on the right ordinate in Fig. 4(a).

The reflection curves for gradient crystals have been calculated recently by a transfer-matrix method (Liss, 1994). Fig. 4(b) shows calculated curves based on linear gradient crystals where the widths at half-maximum correspond to the experimental data shown in Fig. 4(a). The central curve belongs to the perfect crystal without gradient and reaches a peak value of 50%. Already the intensity for small gradients rises quickly to 100%. This is explained by the loss of *Pendellösung* oscillations due to the lattice gradient: while propagating through the crystal, intensity is scattered from the primary beam to the Bragg diffracted beam. For a gradient crystal, the wave field propagates into a crystal volume of different lattice spacing, and the reflection condition is no longer fulfilled. Thus, intensity cannot be reflected back any more and the reflectivity may rise to a maximal value of 100%. Indeed, the reflection curves in Fig. 4(a) measured on the excited crystals match this behavior quite well: first, the peak value increases by about a factor of 2, and then the line width broadens developing a plateau of total reflection. At higher excitation levels, however, the peak value decreases. Note, however, that the integrated intensity continues to rise further, as seen from the markers in Fig. 7. The dynamically calculated values for intensity gains are shown by the continuous

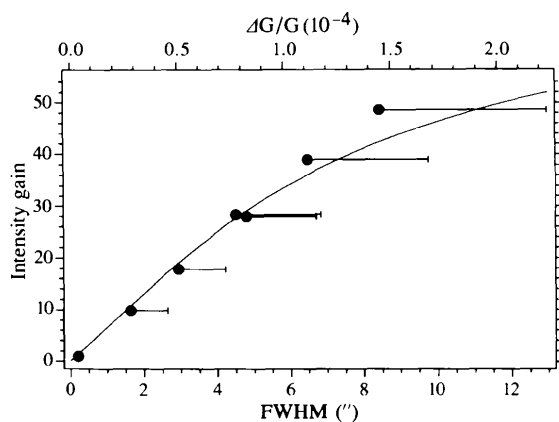


Fig. 7. The circular markers show integrated intensity gains as a function of the full width at half-maximum (FWHM) of the curves displayed in Fig. 4(a). The continuous line is a calculated gain factor based on a crystal with a linear gradient. The bars extending to the right denote the intrinsic widths of the wings of the rocking curves, which should be considered for the amplitudes of lattice strain, represented on the top axis.

line with a maximum value of 80 as derived from the kinematical limit. This is explained by comparing the *Pendellösung* period, Δ_0 , with the total thickness of the crystal. In the present case, $\Delta_0 = 0.393$ mm, and the crystal thickness $D = 9.93$ mm, *i.e.* 25 times the *Pendellösung* period. One layer of thickness Δ_0 is needed to fully build up a rocking curve limited by primary extinction. For a crystal of 9.93 mm thickness, a reflectivity of 100% can only be maintained up to a gain factor of 25 for the integrated intensity. Higher gain factors for the integrated reflectivity can still be obtained by entering the range of kinematical reflection which allows intensity gains of π times the factor 25. However, the value for the plateau will become reduced as observed in Fig. 4(a). This behavior is modeled in Fig. 4(b), where the experimental full widths at half-maximum have been used as the only input parameters. These theoretical curves show a deviation from the 100% plateau value at smaller deformation levels in favor of a box-shaped reflection curve. The intensity is more uniformly distributed over the reflection range than observed for the experimental profiles, where the intensity is more concentrated in the center and the slopes of the edges decrease much slower.

In Laue geometry, the full width at half-maximum of the rocking curve is directly proportional to the utmost widening of the reciprocal-lattice vector and thus to the atomic displacement amplitude of the ultrasonic wave. Thus, a second scale for the abscissa can be drawn as shown at the top of the graph in Fig. 7, such that the intensity profiles reflect the distribution of reciprocal-lattice vectors. In the present case, the wings have an intrinsic width which relates to the specific distribution of the lattice vectors. We consider this by determining the intersection of the tangent in the point of inflection with the abscissa. From this we obtain the peak-to-peak amplitudes, which reach up to 2.2×10^{-4} .

For high sound excitation, the experimental integrated intensities exceed the theoretical values calculated from dynamical theory. This indicates that there exists an incoherent contribution from kinematical diffraction. The experimental intensity gain being higher than expected means that more lattice faults are in the crystal than modeled.

5. Conclusions and outlook

The bulk strain field of the longitudinal ultrasonic wave in an Si single crystal has been measured. Its direction is along the [111] crystal axis and the peak-to-peak value reaches 2.2×10^{-4} , and thus the peak-to-peak amplitude of the atomic displacement is 210 Å.

Integrated intensity gains up to 50 have been achieved. This factor was constrained by the limits of the high-frequency amplifier and not by the material or heat-load problems. The maximum value of the intensity gain is estimated from the comparison of the

extinction length, Δ_0 , to the absorption length, A_0 . With A_0 characterizing the maximal thickness seen by the radiation and Δ_0 being needed to build up interference to 100% reflectivity, the maximum intensity gain is of the order of A_0/Δ_0 . Thus, all extinction-limited monochromators like silicon are suitable for this technique, whereas absorption-limited materials like lead crystals for low-energy X-rays should be discarded. The potential application of an ultrasonically excited crystal is the monochromatization in X-ray and neutron optics. The reflection curves can be tuned instantaneously by a simple electronic set-up whenever diffraction properties close to an ideal crystal have to compromise with the intensity. In addition, the broad and plateau-shaped form of the reflection curve of an ultrasonically excited analyzer crystal could be applied to mechanically follow the Bragg condition in energy-dispersive scans, such as in DAFS or interferometry experiments when the analyzer serves for background and harmonics suppression. Clearly, the positioning of a crystal within 5" is much easier than within 0.1" or less.

The present results may also be of relevance for a novel kind of Bragg optical element where the inclination of the reciprocal-lattice-vector distribution plays an important role. Phase space elements need to be engineered for optimum performance of an instrument. For example, Fig. 8 illustrates how an inclined distribution of scattering vectors, \mathbf{G} , reflects the accepted phase space element, A , towards a hypothetical desired, horizontally oriented phase space element, R . As discussed elsewhere (Liss & Magerl, 1994), arbitrarily oriented phase space elements play an important role in multocrystal diffractometry apart from the non-dispersive set-up. The constraints on a reflected phase space element should be relaxed as much as possible without decreasing the desired resolution in the dimension probed for. Here again, the tuneability of ultrasonically excited crystals plays an important role. Imagine a sophisticated monochromator cut with transducers exciting ultrasonic waves in two different directions. The superposition of these waves would allow the rotation of the reciprocal-lattice-vector distribution by electronically varying the amplitudes and phases of both transducers.

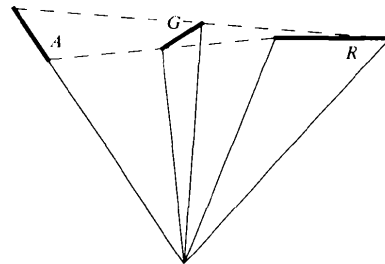


Fig. 8. An example demonstrating how an accepted phase space element, A , is reflected by an inclined reciprocal-lattice vector distribution, G , towards a horizontally oriented element, R .

References

- Alefeld, B. (1969). *Z. Phys.* **228**, 454–464.
- Hock, R., Vogt, T., Kulda, J., Mursic, Z., Fuess, H. & Magerl, A. (1993). *Z. Phys.* **B90**, 143–153.
- Kulda, J., Vrána, M. & Mikula, P. (1988). *Physica (Utrecht)*, **B151**, 122–123.
- Liss, K.-D. (1994). Dissertation, RWTH Aachen, Aachen, Germany.
- Liss, K.-D. & Magerl, A. (1994). *Nucl. Instrum. Methods*, **A338**, 90–98.
- Magerl, A., Liss, K.-D., Doll, C., Madar, R. & Steichele, E. (1994). *Nucl. Instrum. Methods*, **A338**, 83–89.
- Magerl, A., Liss, K.-D., Hastings, J. B., Siddons, D. P., Neumann, H.-B., Poulsen, H. F., Rütt, U., Schneider, J. R. & Madar, R. (1995). *Europhys. Lett.* **31**(5–6), 329–334.
- Neumann, H.-B. (1991). Internal Report 91–06, HASYLAB, DESY, Germany.
- Neumann, H.-B., Rütt, U., Bouchard, R., Schneider, J. R. & Nagasawa, H. (1994). *J. Appl. Cryst.* **27**, 1030–1038.
- Rauch, H. & Petrascheck, D. (1976). *Grundlagen für ein Laue-Neutroneninterferometer Teil 1: Dynamische Beugung*, Report AIAU 74405b, Atominstitut der Österreichischen Universitäten, Austria.
- Rauch, H. & Petrascheck, D. (1978). *Neutron Diffraction*, edited by H. Dachs, pp. 303–351. Berlin/Heidelberg/New York: Springer-Verlag.
- Rustichelli, F. (1972). *Neutron Inelastic Scattering*, pp. 697–711. Vienna: International Atomic Energy Agency.
- Suortti, P. & Tschentscher, T. (1995). *Rev. Sci. Instrum.* **66**(2), 1798–1801.
- Taupin, D. (1964). *Bull. Soc. Fr. Minéral. Crystallogr.* **87**, 469–511.
- Tschentscher, T., Buslaps, T., Fajardo, P., Honkimäki, V., Kretschmer, M., Liss, K.-D., Mauro, A., McCarthy, J., Renier, M., Shukla, A. & Suortti, P. (1996). *ESRF Newsletter*, **25**, 30–33.
- Zachariasen, W. H. (1945). *Theory of X-ray Diffraction in Crystals*. London: John Wiley and Sons.